*J. Fluid Mech.* (2002), *vol.* 472, *pp.* 153–166.  
DOI: 10.1017/S0022112002002288 Printed in the United Kingdom

# Fission of collapsing cavitation bubbles

By CHRISTOPHER E. BRENNEN

Department of Mechanical Engineering, California Institute of Technology, Pasadena, CA 91125, USA

(Received 27 March 2001 and in revised form 19 June 2002)

High-speed observations clearly show that though a collapsing cavitation bubble approaches its minimum size as a coherent single volume, it usually reappears in the first rebounding frame as a cloud of much smaller bubbles or as a highly distorted single volume. This paper explores two mechanisms that may be responsible for that bubble fission process, one invoking a Rayleigh–Taylor stability analysis and the other using the so-called microjet mechanism. Both approaches are shown to lead to qualitatively similar values for the number of fission fragments and the paper investigates the flow parameters that effect that number. Finally, the additional damping of the Rayleigh–Plesset single-bubble calculation caused by the fission process is investigated; it is shown that the fission damping dominates other contributions normally considered and is consistent with the number of collapses and rebounds that are observed to occur in experiments.

## 1. Introduction

Rayleigh–Plesset calculations for cavitation bubbles are now commonly embedded in efforts to simulate cavitating flows computationally . The implicit assumption is that the bubble remains sufficiently spherical for this equation to represent its dynamic volumetric behaviour adequately. When the latter is compared with experimental observations (see, for example, Kuhn de Chizelle, Ceccio & Brennen 1995), there are many respects in which this approximation proves acceptable, particularly during the growth of the bubble to its maximum size and the initial part of the collapse phase. However, most high-speed observations of the collapse show that the bubble fissions during passage through its minimum volume (figure 1) and, thereafter, the Rayleigh–Plesset analysis fails to predict the dynamic behaviour accurately. In part, this is because the Rayleigh–Plesset equation fails to represent the energy dissipation associated with the fission process. As a consequence, the number and strength of the rebounds observed in the experiments are much smaller than predicted by the calculations.

This paper attempts to model the fission process in order to generate modifications to the Rayleigh–Plesset equation which would handle the fission process, albeit approximately. Two mechanisms that may be responsible for that bubble fission process are explored, one invoking a Rayleigh–Taylor stability analysis and the other centred on the so-called microjet mechanism of collapse. Both approaches are shown to lead to qualitatively similar values for the number of fission fragments. Then, the energy dissipation or absorption due to those fission processes is explored and this leads, in turn, to an exploration of the effective damping that might be included in the Rayleigh–Plesset model in order to model the energy attenuation which the fission process implies.

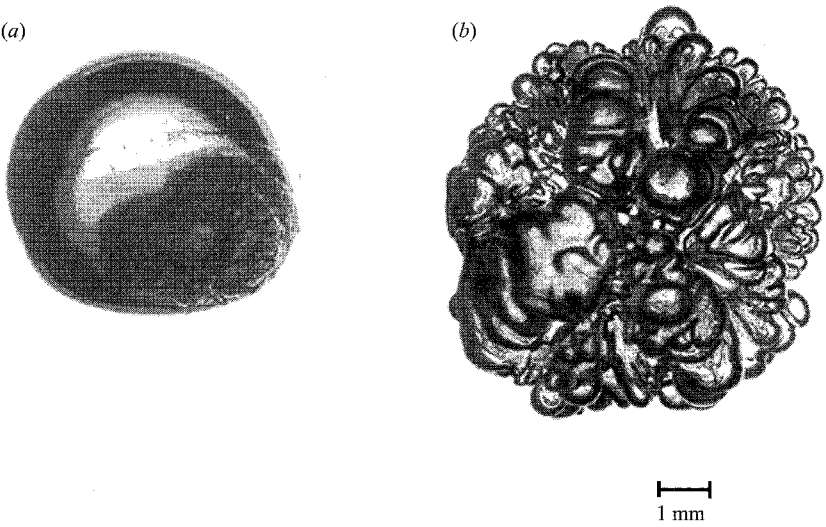


FIGURE 1. Photographs of an ether vapour bubble in glycerol (*a*) before and (*b*) after the first collapse (reproduced with permission from Frost & Sturtevant 1986).

The paper is focused on the bubble dynamics that are typical of most (though not necessarily all) practical bubbly cavitating flows. In such flows, gas-filled nuclei in the size range 5–30 μm grow explosively when they are convected into a low-pressure region (below vapour pressure) and then collapse as they are convected out into regions of higher pressure. We exclude the rather special bubble dynamics manifest in sonoluminesence experiments (see, for example, Hilgenfeldt *et al.* 1998) that involve smaller nuclei (and much greater time rates of change). In those special circumstances, bubbles remain spherical down to much smaller size and thus produce gas compression effects that require the inclusion of liquid compressibility and other effects which are omitted from the present analysis. Liquid compressibility effects become important in bubble collapse when the Mach number of the interface velocity approaches about 0.3. As shown by the example in § 5, bubble fission in most cavitating flows begins long before such Mach numbers occur. Consequently, the present analysis omits liquid compressibility effects. Another measure of assurance that the incompressible liquid form of the Rayleigh–Plesset equation is appropriate to the present calculations is provided by the comparisons of the calculated and measured noise emissions from travelling cavitation bubbles presented by Kuhn de Chizelle *et al.* (1995). There it is shown that though the measured noise emission for larger bubbles is substantially less than predicted by the incompressible Rayleigh–Plesset equation, this discrepancy is caused by bubble distortion and the results agree for smaller bubbles for which the distortion is much less.

## 2. Collapse relations

Before analysing possible fission processes, it is necessary to detail an approximate analytical model that includes the essential features of the growth and collapse of a cavitating bubble as it passes through a low-pressure region in the flow. For this purpose, the classical Rayleigh–Plesset model is used. For simplicity, it is assumed that the liquid temperature is low enough for thermal effects to be neglected, that the mass of non-condensable gas in the bubble remains constant and that the behaviour of that gas can be represented by a polytropic constant, $k$. With the above assumptions,

the Rayleigh–Plesset equation (see, for example, Brennen 1995) connecting the time-dependent bubble radius, $R(t)$, to the pressure in the liquid, $p_\infty(t)$, becomes

$$\frac{p_V - p_\infty(t)}{\rho} + \frac{p_{Go}}{\rho}\left\{\frac{R_o}{R}\right\}^{3k} = R\ddot{R} + \tfrac{3}{2}(\dot{R})^2 + \frac{4\mu_e \dot{R}}{\rho R} + \frac{2S}{\rho R}, \tag{2.1}$$

where $p_V$ is the vapour pressure at the prevailing temperature, $p_{Go}$ is the partial pressure of non-condensable gas in the initial cavitation nucleus, $\rho$ and $S$ are the liquid density and the surface tension, the overdot denotes $\mathrm{d}/\mathrm{d}t$ and, for the moment, $\mu_e$ can be thought of as the liquid viscosity.

For the purposes of the present investigation, consider the evolution of a single cavitation nucleus of radius $R_o$ initially at equilibrium at the initial liquid pressure $p^i_\infty$. The initial partial pressure of gas is given by

$$p_{Go} = p^i_\infty - p_V + \frac{2S}{R_o}. \tag{2.2}$$

This nucleus is then subjected to an episode in which the liquid pressure is decreased below the vapour pressure, $p_V$, causing explosive cavitation growth of the bubble to a radius much larger than $R_o$. The ambient pressure eventually increases again, causing the bubble to collapse violently. Such a scenario is typical of travelling bubble cavitation whether in a pump, turbine, ship's propeller, artificial heart valve or many other situations in which cavitation occurs.

Clearly, the nonlinearities in the Rayleigh–Plesset equation severely limit progress toward exact solutions. Here, because of the approximations made later in the development of the theory, it would not be consistent to pursue numerical solutions (even though they are now commonplace). Rather, an approximate analytical approach is developed that is sufficient for present purposes.

The analysis will focus on that very brief instant at the heart of the collapse when the bubble radius becomes very much smaller than $R_o$. Assuming that, during that brief period, the liquid pressure is roughly constant at some value, $p^c_\infty$, and, neglecting the viscous term, the Rayleigh–Plesset equation can be integrated once to obtain

$$(\dot{R})^2 = \frac{K}{R^3} - \frac{2(p^c_\infty - p_V)}{3\rho} - \frac{2p_{Go}}{3\rho(k-1)}\frac{R_o^{3k}}{R^{3k}} - \frac{2S}{\rho R}, \tag{2.3}$$

where $K$ is an integration constant. This constant can be approximately evaluated by relating it to the maximum size of the bubble, $R_{max}$, at which $\dot{R} = 0$. The reason this is only approximate is that the maximum size may well be achieved when the pressure is significantly different from $p^c_\infty$; but accepting this approximation and assuming that $R_{max} \gg R_o$ and that $k > 1$,

$$K \approx 2(p^c_\infty - p_V)R^3_{max}/3\rho. \tag{2.4}$$

Of course, $R_{max}$, will not be known *a priori*. For future purposes, it is therefore useful to define a typical duration for the reduced pressure interval (for the growth process), $t_R$, and a typical tension, $p_V - p^m_\infty$, under which growth occurs. Since the growth rate during this phase is dominated by the equivalent of the second term on the right-hand side of (2.3), it follows that the maximum bubble size can be estimated to be

$$R_{max} = \left\{\frac{2(p_V - p^m_\infty)t_R^2}{3\rho}\right\}^{1/2}. \tag{2.5}$$

Now examine the behaviour manifest by (2.3) during the heart of the collapse when $R \ll R_o$. Then, the two important terms on the right-hand side imply that

$$(\dot{R})^2 \to \frac{K}{R^3} - \frac{2p_{Go}}{3\rho(k-1)}\frac{R_o^{3k}}{R^{3k}}, \tag{2.6}$$

and that

$$R\ddot{R} \to \frac{k}{(k-1)}\frac{p_{Go}}{\rho}\frac{R_o^{3k}}{R^{3k}} - \frac{3K}{2R^3}. \tag{2.7}$$

From (2.6), it follows that the minimum size reached by the bubble is

$$\frac{R_{min}}{R_o} = \left\{\frac{2R_o^3 p_{Go}}{3\rho(k-1)K}\right\}^{1/3(k-1)} = \left\{\frac{p_{Go}}{(k-1)(p_\infty^c - p_V)}\right\}^{1/3(k-1)}\left\{\frac{R_o}{R_{max}}\right\}^{1/(k-1)}. \tag{2.8}$$

Note that, when $p_{Go}$ is small, $R_{min}$ can be very small indeed and that the maximum and minimum bubble sizes are inversely related.

Another moment in the collapse process which is important to the present analysis is the moment at which the acceleration, $\ddot{R}$, changes from negative to positive. This will be referred to as the beginning of the rebound. From (2.7), it follows that this occurs when the radius takes the value, $R_*$, where

$$R_* = (k)^{1/3(k-1)}R_{min}, \tag{2.9}$$

which for any reasonable value of $k$ is close to $\frac{4}{3}R_{min}$. Moreover, the velocity at this moment is given by

$$\dot{R}_* = \left\{\frac{(k-1)}{k}\frac{K}{R_*^3}\right\}^{1/2}. \tag{2.10}$$

For reasons discussed below, our focus will be on the very brief interval of time following $R = R_*$ and up to and somewhat beyond $R = R_{min}$. Since $R_*/R_{min}$ is close to unity, (2.6) can be integrated approximately to obtain $R$ as a function of time during this interval:

$$\frac{R}{R_{min}} = 1 + \left\{\frac{3(k-1)K}{4R_{min}^5}\right\}t^2 + \cdots, \tag{2.11}$$

where the time origin, $t = 0$, is chosen to be at $R = R_{min}$. It also follows from (2.7) that the critical time interval, $-t_* < t < +t_*$, in which $R < R_*$ is defined by

$$t_*^2 \approx \frac{4R_{min}^5}{9(k^2-1)K}. \tag{2.12}$$

This completes the exploration of the 'global motion', $R(t)$, which will be necessary for the evaluations of the following sections.

However, before considering fission processes, it is convenient to parameterize the above results in the following way. First, a Thoma cavitation number, $\sigma$, is defined; this describes how close the inlet pressure is to the vapour pressure. Also, a non-dimensional pressure distribution characteristic, $\alpha$, is defined as follows:

$$\sigma = \frac{(p_\infty^i - p_V)}{(p_\infty^i - p_\infty^m)}, \quad \alpha = \frac{(p_\infty^c - p_\infty^m)}{(p_\infty^i - p_\infty^m)}. \tag{2.13}$$

The parameter $\alpha$ will be a characteristic of the geometry of the flow regardless of the vapour pressure and will often take a value of the order of unity. Then, the surface

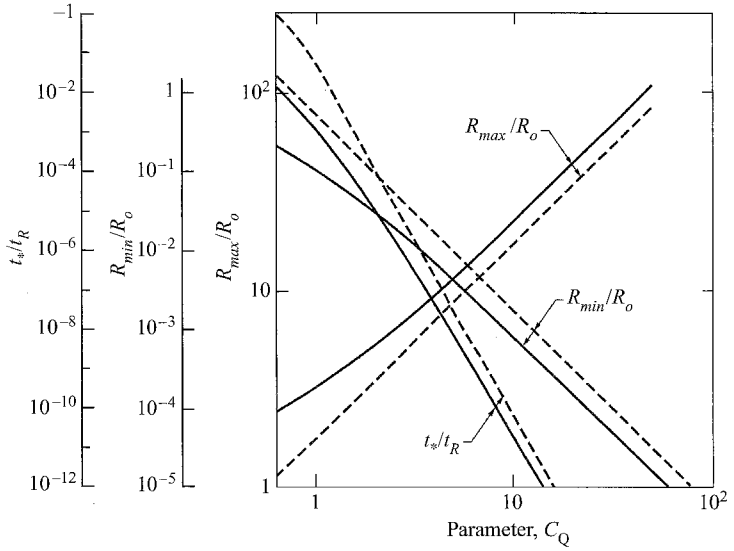


FIGURE 2. Typical comparisons between ——, the exact values and – – –, the approximate expressions for $R_{max}/R_o$, $R_{min}/R_o$, and $t_*/t_R$ for $k = 1.4$, $\alpha = 1$, $\sigma = 0.5$ and sufficiently small values of the surface tension and viscosity.

tension, $S$, and the residence time, $t_R$, are conveniently represented by the parameters:

$$R_o^* = \frac{R_o(p_\infty^i - p_\infty^m)}{S}, \quad C_P = \frac{t_R}{R_o}\left\{\frac{2(p_\infty^i - p_\infty^m)}{3\rho}\right\}^{1/2}. \tag{2.14}$$

Note that in (2.13) and (2.14), the pressure difference $(p_\infty^i - p_\infty^m)$ has been uniformly used as one of the non-dimensionalizing factors.

In addition, a combination parameter that will appear in several places in the results ahead, is defined:

$$C_Q = C_P(k-1)^{1/3}(\alpha - 1 + \sigma)^{1/3}(1-\sigma)^{1/2}. \tag{2.15}$$

Note for future purposes that

$$\frac{R_{max}}{R_o} = C_P(1-\sigma)^{1/2}, \quad \frac{R_{min}}{R_o} = (\sigma + 2/R_o^*)^{1/3(k-1)}C_Q^{-1/(k-1)},$$

$$K = \frac{2R_o^3C_Q^3(p_\infty^i - p_\infty^m)}{3\rho(k-1)}. \tag{2.16a–c}$$

To provide some illustration of the accuracy of these approximations, numerical integrations of the Rayleigh–Plesset equation, (2.1), were carried out in order to compare the exact values of $R_{max}/R_o$, $R_{min}/R_o$ and $t_*/t_R$ with the values given by the above approximations. For this purpose, a Heaviside function pressure/time history was used in which the pressure was suddenly decreased from $p_\infty^i$ to $p_\infty^m$ and then increased abruptly again to $p_\infty^i$ after a time $t_R$ (thus the parameter $\alpha = 1$). Such calculations were performed for a typical $k = 1.4$, for various cavitation numbers, $\sigma$, and for various values of the parameter $C_Q$ which effectively sets the dimensionless duration of the low-pressure episode. Provided the surface tension and viscosity are small enough (as is typically the case) they do not affect the results in a major way. Then, the comparisons shown in figure 2 are typical and the approximations are sufficiently accurate for the purposes of this paper.

## 3. Stability to spherical harmonic distortion

The stability of cavitating bubbles to non-spherical disturbances has been investigated analytically by Birkhoff (1954), Plesset & Mitchell (1956), Brennen (1995) among others. These analyses examined the spherical equivalent of the Rayleigh–Taylor instability. If the inertia of the gas in the bubble is assumed to be negligible, then the amplitude, $a(t)$, of a spherical harmonic distortion of order $n$ ($n > 1$) is governed by the equation:

$$\frac{\mathrm{d}^2a}{\mathrm{d}t^2} + \frac{3}{R}\frac{\mathrm{d}R}{\mathrm{d}t}\frac{\mathrm{d}a}{\mathrm{d}t} - \left\{\frac{(n-1)}{R}\frac{\mathrm{d}^2R}{\mathrm{d}t^2} - (n-1)(n+1)(n+2)\frac{S}{\rho R^3}\right\}a = 0. \tag{3.1}$$

Note that the coefficients require knowledge of the global dynamic behaviour, $R(t)$. The fact that they are not constant in time causes departure from the equivalent Rayleigh–Taylor instability for a plane boundary. However, the coefficient of $a$ within the brackets, $\{\}$, of (3.1) is not greatly dissimilar from the case of the plane boundary in the sense that instability is promoted when $\ddot{R} > 0$ and surface tension has a stabilizing effect. Plesset & Mitchell (1956) examined the particular case of a vapour/gas bubble initially in equilibrium that is subjected to a step function change in the pressure at infinity. Later calculations by Brennen (1995), incorporated the effect of the non-condensable gas in the bubble. The effect of the gas is essential for present purposes since its compression causes the rebound and therefore the instability that is addressed here.

It is clear from (3.1) that the most unstable circumstances occur when $\dot{R} < 0$ and $\ddot{R} \geqslant 0$. These conditions are met following the beginning of the rebound (as defined earlier) and result in very rapid growth in non-spherical distortion. I submit that this leads to the very rapid disintegration of the bubble and its metamorphosis into the cloud of smaller bubbles that is seen in experiments to emerge from the collapse of the bubble. The growth rate of the distortions is controlled by the magnitude of the term in the brackets, $\{\}$, in (3.1). The larger the value of this term, the greater the growth rate. Note that $n$ occurs only in this term and that the functional dependence on $n$ has the form

$$(n-1)\{\Gamma - (n+1)(n+2)\} \quad \text{where} \quad \Gamma = \rho R^2\ddot{R}/S. \tag{3.2}$$

It follows that as long as $\Gamma$ is positive, there will be a particular value of $n$ (denoted by $n_m$) for which the term has a positive maximum. This mode of distortion is expected to dominate and therefore to play a role in determining the number of fission bubbles. (It is noted that Shepherd (1980) follows a qualitatively similar argument in an effort to predict the wavelengths of surface distortion seen on the bubbles in the experiments from which figures 1 and 4 are taken.)

One complicating factor is that $\Gamma$ will vary with time within the unstable interval increasing from zero at $t = -t_*$ to a maximum $\Gamma_m$ when $R = R_{min}$ and decreasing again to zero at $t = t_*$. Clearly, however, $\Gamma_m$ is a representative value and, using the results of § 2, can be written in terms of the parameters defined in that section:

$$\Gamma_m = \frac{R_o^* C_Q^{(3k-1)/(k-1)}}{(\sigma + 2/R_o^*)^{2/3(k-1)}}. \tag{3.3}$$

Then, taking $\Gamma_m$ as the characteristic value of $\Gamma$, the most unstable mode follows directly from (3.2) as

$$n_m = \tfrac{1}{3}\{(7 + 3\Gamma_m)^{1/2} - 2\}, \tag{3.4}$$

and, provided $n_m \gg 1$,

$$n_m \approx \{\tfrac{1}{3}\Gamma_m\}^{1/2} = \frac{(R_o^*)^{1/2} C_Q^{(3k-1)/2(k-1)}}{3^{1/2}(\sigma + 2/R_o^*)^{1/3(k-1)}}. \tag{3.5}$$

Note that $n_m \approx (\frac{1}{3}\Gamma_m)^{1/2}$ is functionally similar to the most unstable surface distortion wavelength prediction included in the analysis of Shepherd & Sturtevant (1982).

Given the most unstable Rayleigh–Taylor mode, the next problem is to estimate the number of fission fragments which that mode might produce. Assuming that the fission fragment size is directly related to the wavelength of the distortion on the surface of the whole bubble, a crude estimate would be that the fragment radius, $R_F$, would be given roughly by $R_F = R/n_m$. Then, if the original volume is equally divided amongst these fragments, it follows that the number of fission fragments is $n_m^3$.

Discussion of this result is delayed until an alternative approach is examined.

## 4. Jet breakup

The results at the end of the last section assumed a particular model of bubble fission. In other circumstances, it is observed that a bubble collapsing close to a wall or free-surface forms a re-entrant jet which shatters the bubble into many fragments when the jet impacts the other side of the bubble surface. In this section an estimate is made of the number of fission fragments that would result from this mode of bubble disintegration. To do so crudely, the size of the bubbles that survive such a violent process is estimated to be that size for which the surface tension forces holding the fission fragment together are roughly equal to the shear forces tearing it apart. The shear rates involved could be estimated as $\gamma = \dot{R}/R$ at the beginning of the rebound and, from (2.9) and (2.10), $\dot{R}$ can be estimated as $\dot{R}_*$ where

$$\dot{R}_*^2 = \frac{\{R_o C_P/t_R\}^2 \{C_Q/k^{1/3}\}^{3k/(k-1)}}{\{\sigma + 2/R_o^*\}^{1/(k-1)}}. \tag{4.1}$$

To estimate the fission fragment size, $R_F$, the typical surface tension force, $2\pi R_F S$, is then equated to the typical shearing force, $6\pi\mu\gamma R_F^2$ so that $R_F = S/3\mu\gamma$. It follows that the number of fission fragments would be $n_j^3$ where

$$n_j = \frac{R_*}{R_F} = \frac{3\mu\dot{R}_*}{S}. \tag{4.2}$$

This is clearly a function of the previously used parameters $\sigma$, $\alpha$, $k$, $R_o^*$ and $C_P$, as well as a Reynolds-number-like viscous parameter, $C_\mu$:

$$C_\mu = \frac{R_o\{\rho(p_\infty^i - p_\infty^m)\}^{1/2}}{\mu}. \tag{4.3}$$

Then, (4.2) can be written as

$$n_j = \frac{6^{1/2} R_o^* \{C_Q/k^{1/3}\}^{3k/2(k-1)}}{C_\mu(\sigma + 2/R_o^*)^{1/2(k-1)}}. \tag{4.4}$$

The shearing force, $6\pi\mu\gamma R_F^2$, used in deriving this result is a low-Reynolds-number formulation and requires that $\rho\dot{R}_* R_*/\mu \ll 1$. If, on the other hand, $\rho\dot{R}_* R_*/\mu \gg 1$, an appropriate estimate of the shearing force would be $\pi\rho\gamma^2 R_F^4$. Then it would

follow that

$$n_j = \frac{R_*}{R_F} = \left\{ \frac{\rho \dot{R}_*^2 R_*}{2S} \right\}^{1/3}, \tag{4.5}$$

and, in terms of the defined parameters,

$$n_j = \frac{(R_o^*)^{1/3} \{C_Q/k^{1/3}\}^{(3k-1)/3(k-1)}}{3^{1/3}(\sigma + 2/R_o^*)^{2/9(k-1)}}. \tag{4.6}$$

Clearly, fragmentation as a result of the formation of a re-entrant jet is a very complex process. Equation (4.6) is admittedly a crude and heuristic estimate of the resulting fragment size. In the next section, the applicability and consequences of (4.4) and (4.6) are considered.

## 5. Fission fragments

In assessing the results of the last two sections, namely (3.5), (4.4) and (4.6) for the number of fission fragments, note that all three results have similar forms. This is because they all involve fission forces which are inertial in origin and a resistance to fission governed by surface tension. Moreover, since $\sigma$ is often of order unity, the magnitude of $n_m$ or $n_j$ is primarily determined by the numerator and is therefore a function of $R_o^*$ and $C_Q$ (or, effectively, $C_P$), though $C_\mu$ also appears in (4.4). Concentrating on those numerators involving $R_o^*$ and $C_Q$, note that $n_m$ and $n_j$ sensibly decrease with increasing $S$. The variation with nuclei size is more complex and requires consideration of the factor $(\sigma + 2/R_o^*)$ in the denominators. For very small nuclei sizes such that $R_o^* \ll 2/\sigma$ the number of fission fragments increases with the nuclei size (provided $k$ takes some reasonable number). However, for larger nuclei such that $R_o^* \gg 2/\sigma$ the number of fission fragments decreases as the nuclei size increases. This slightly non-intuitive trend occurs because the maximum bubble size becomes essentially independent of the nuclei size; however, the larger nuclei contribute more non-condensable gas to the collapse and the collapse is therefore less violent, leading to fewer fission fragments.

It is also appropriate at this point to comment on the low bubble Reynolds-number result, (4.4). It is fairly easy to demonstrate that if the viscous terms dominate the inertial terms and lead to (4.4) rather than (4.6) then the viscous terms in the Rayleigh–Plesset equation itself should have been included in the analysis of §2. Since they were not so included, it follows that (4.4) is of dubious validity. Moreover, in many of the cases of practical interest, the contribution of the viscous term to the overall bubble dynamics described in §2 is small. Consequently, in the interest of brevity, the low bubble Reynolds-number result, (4.4), will not be pursued any further.

The results in (3.5) and (4.6) for $n_m$ and $n_j$ will now be illustrated with some numerical examples. In figure 3, values for $n_m$ and $n_j$ from (3.5) and (4.6) are plotted against the dimensionless nuclei size, $R_o^*$, for various values of the parameter, $C_Q$, and the cavitation index, $\sigma$. Note again the similarity in the results for the two fission models, the result, as mentioned above, of similar physical origins for the forces causing and resisting fission.

For a typical surface tension, $S$, of $0.07\,\mathrm{kg\,s^{-2}}$ and a typical pressure difference, $(p_\infty^i - p_\infty^m)$, of $10^5\,\mathrm{kg\,m^{-1}\,s^{-1}}$, nuclei of radii, $R_o$, ranging from 1 μm to 100 μm would yield $R_o^*$ values ranging from 1.4 to 140, roughly in the middle of the horizontal scale. Moreover, cavitation indices in the range used in the figures are commonly experienced. Perhaps the greatest uncertainity lies in estimating typical values of $C_Q$

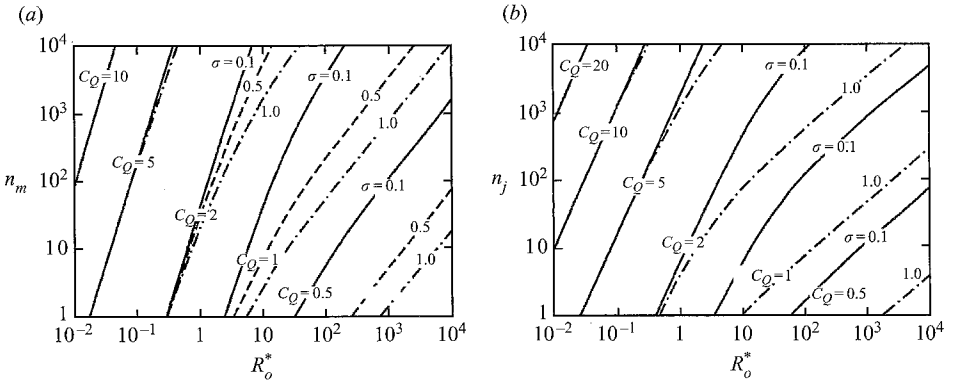


FIGURE 3. (*a*) Values of $n_m$ from the Rayleigh–Taylor instability analysis. (*b*) Values of $n_j$ from the re-entrant jet breakup analysis. Both plotted against $R_o^*$ for $k = 1.4$ and various values of the parameter, $C_Q$, and the cavitation number, $\sigma$.

occurring in practice. The simplest way to estimate this is to use (2.16*a–c*). Common values of $R_{max}/R_o$ range from 10 up to 100 and higher and this provides an estimate of $C_P$. Equation (2.15) suggests that $C_Q$ will typically be about an order of magnitude smaller than $C_P$ and this leads to an estimate of $C_Q$ of order unity or greater. Figure 3 indicates that for $C_Q = 1$ the smaller nuclei may lead to collapses without fission if the cavitation number is large enough. However, large nuclei at lower cavitation numbers will lead to breakup into large numbers of fission fragments.

(We note that the bubble wall velocities at the beginning of rebound in the above examples are of the order of 3–10 m s$^{-1}$. The Mach numbers are therefore much smaller than those at which liquid compressibility would become important.)

## 6. Some comparisons with observations

While many of the photographs of cavitation bubbles before and after the first collapse (for example, Lauterborn & Bolle 1975; Tomita & Shima 1990) show that the bubble has fissioned into many fragments, the photographs rarely have the kind of resolution that would allow a count of the number of those fragments. On the other hand, though they are not normal cavitation bubbles, the photographs of Frost & Sturtevant (1986) showing the breakup of ether vapour bubbles in glycerol are of sufficient resolution to allow comparison with the present analysis.

Frost & Sturtevant (1986) (see also, Shepherd & Sturtevant 1982; Shepherd 1980; Frost 1985) allowed drops of ether in gycerol to evapourate explosively and then examined the surface appearance as the bubble oscillated. In addition, they measured the pressures radiated as a result of these oscillations. Sample photographs just after the first collapse are shown in figure 4. Using these photographs, the individual bubbles observable on the half-surface facing the camera were counted. Doubling that number to account for the back surface yielded values of 320, 400 and 410, respectively, for the three cases. In the framework of § 3, this number should correspond to $n_m^2$ and hence the photographs indicate $n_m \approx 20$.

To compare with the theory of § 3, note that the pressure radiated from an oscillating bubble has an amplitude, $\tilde{p}$, given roughly by

$$\tilde{p} = \frac{\rho}{4\pi\mathscr{R}} \frac{\mathrm{d}^2 V}{\mathrm{d}t^2} \approx \frac{\rho R^2}{\mathscr{R}} \frac{\mathrm{d}^2 R}{\mathrm{d}t^2}, \tag{6.1}$$

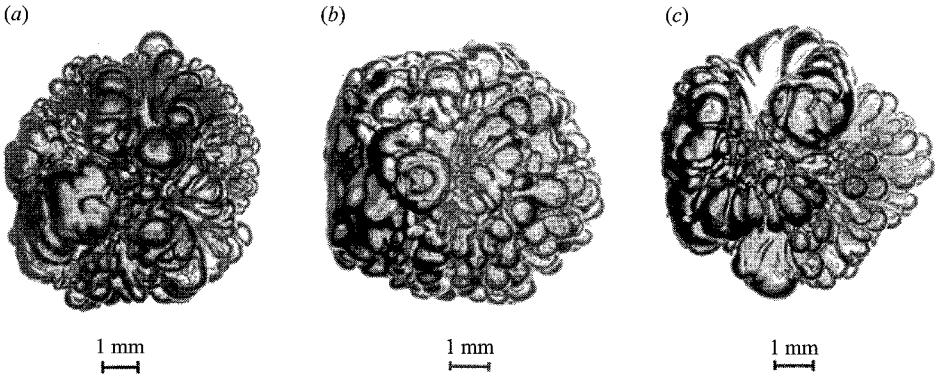


FIGURE 4. Photographs of ether vapour bubbles in glycerol after the first bubble collapse (reproduced with permission from Frost 1985).

where $V$ and $R$ are the volume and radius of the bubble and $\mathscr{R}$ is the distance from the bubble centre to the point of pressure measurement (see Brennen 1995). Substituting for $R^2\mathrm{d}^2R/\mathrm{d}t^2$ in (3.2) and using the approximation in (3.5) yields

$$n_m = \left\{\frac{\Gamma_m}{3}\right\}^{1/2} \approx \left\{\frac{\mathscr{R}|\tilde{p}|}{3S}\right\}^{1/2}, \tag{6.2}$$

where $|\tilde{p}|$ is the amplitude of the radiated pressure. From the pressure traces given by Frost (1985), the values of $|\tilde{p}|$ for the three photographs in figure 4 were estimated to be $6 \times 10^4\,\mathrm{kg\,m^{-1}\,s^{-2}}$. With this, $\mathscr{R} = 6\,\mathrm{mm}$ and $S = 0.07\,\mathrm{N\,m^{-1}}$ (6.2) then yields $n_m = 41$.

Though the evidence is limited, the qualitative agreement between the theoretical value of $n_m = 41$ and the experimental values around $n_m = 20$ is encouraging. Note that Shepherd (1980) found a similar relation between the predicted and observed distortion wavelengths in his analysis of the same experiments. Clearly, however, further comparisons are necessary to validate the theory.

## 7. Effective damping

Calculations of the global dynamics, $R(t)$, which use the Rayleigh–Plesset equation and therefore assume spherical symmetry, require an estimate of the energy dissipation in order to yield realistic results. The dissipation can have a number of physical origins including viscous dissipation in the liquid, thermal effects at the bubble surface and acoustic radiation. In one of the first efforts to summarize these various sources of dissipation, Chapman & Plesset (1971) proposed using an effective viscosity, $\mu_e$, which was the sum of contributions from these various sources in the viscous term of the Rayleigh–Plesset equation. Of course, the consequences of the complex processes associated with thermal and mass diffusion within the liquid and within the gas, do not necessarily conform to the polytropic form assumed by Chapman & Plesset and so a substantial literature subsequently emerged which treated these processes within the context of a spherical bubble geometry (see, for example, Nigmatulin, Khabeev & Nagiev 1981; Prosperetti 1991; Matsumoto & Takemura 1994).

However, when any of these techniques are applied to cavitating bubble dynamics such as are the subject of this paper, estimates of the damping or effective viscosity always produce far larger and more numerous rebounds than are observed

experimentally. It is often remarked that this is because the bubble almost never remains spherical through the first collapse. Experimental observations such as those of Lauterborn & Bolle (1975) and Tomita & Shima (1990) show that though the bubble may remain relatively intact prior to the first collapse, what emerges from that collapse is either a highly distorted bubble mass or a cloud of bubble fragments. The photographs of Frost & Sturtevant (1986) provide particularly good examples of this. Moreover, they observed further fragmentation during subsequent collapses. It seems likely that this fragmentation process dissipates substantial energy and therefore may contribute in a major way to the effective damping of the collapse and rebound cycle. Perhaps this is why the observed number of these cycles rarely exceeds three or four.

In this paper, an attempt has been made to evaluate the mode of breakup of a bubble during the collapse process. As a part of this, it is useful to attempt to identify the energy exchange associated with this fission process. One objective would be to determine whether or not the observed attenuation of the collapse and rebound cycle could be accounted for. The first step is to recall that the viscous term being used in the usual Rayleigh–Plesset equation, (2.1), (where $\mu_e$ is now an effective viscosity that incorporates several mechanisms of dissipation) implies a rate of dissipation of energy given by

$$16\pi\mu_e R(\dot{R})^2. \tag{7.1}$$

If, using the results of § 2, this is integrated over the collapse interval, $-t^* < t < t^*$, an expression for the total energy dissipated during that interval emerges:

$$\frac{64\pi\mu_e}{9}\left\{\frac{R_{min}K(k-1)}{(k+1)^3}\right\}^{1/2}. \tag{7.2}$$

Turning this around, if the energy, $E_D$, dissipated in a collapse as a result of fission were estimated, then the appropriate value of $\mu_e$ that should be used to represent the fission dissipation is

$$\mu_e = \frac{9E_D}{64\pi}\left\{\frac{(k+1)^3}{R_{min}K(k-1)}\right\}^{1/2}. \tag{7.3}$$

The next step is to consider the fission process and to estimate the absorption of energy that occurs during that process. As a part of that process, in the next section, $E_D$ will be connected to the number of fission fragments, $n_m^3$ or $n_j^3$.

## 8. Dissipation mechanisms during fission

There are several mechanisms by which the energy associated with the radial motion may be deflected or dissipated. First, the formation of jets or surface waves will channel kinetic energy in directions in which the energy must end up being dissipated by viscosity as a result of the fluid mixing and turbulence. Secondly, the bubble fragments that emerge from the fission process must necessarily contain more surface free energy than the single bubble prior to collapse. This deflection of energy will clearly also decrease the kinetic energy associated with the volumetric or radial motion and therefore contribute to the damping. Estimates of both of these contributions to the fission damping will now be attempted.

First, the discussion is framed by observing that the kinetic energy, $E$, of a single spherical bubble in an infinite fluid is

$$E = 2\pi\rho\dot{R}^2R^3. \tag{8.1}$$

Specifically, the kinetic energy, $E^*$, at the start of the rebound is

$$E^* = 2\pi\rho R_*^3 \dot{R}_*^2 = 2\pi\rho \frac{(k-1)}{k} K. \tag{8.2}$$

To estimate the kinetic energy which might be dissipated owing to mixing, I suppose that a single microjet penetrates the single bubble just after the beginning of the rebound when $R = R^*$ and achieves a velocity that is some multiple, $C_J$, of $\dot{R}_*$ (the work of Blake & Gibson 1987 and others suggests that $C_J$ may be as high as 10 – see Brennen 1995). Then, if it is assumed that all the kinetic energy, $E_J$, in the jet is dissipated during collapse and that the jet radius is $1/C_J$ of the bubble radius at the beginning of rebound, it would follow that

$$E_J \propto \pi\rho R_*^3 \dot{R}_*^2. \tag{8.3}$$

This simply states that the loss is a fraction of the total kinetic energy at the start of the rebound. Consequently, the radial kinetic energy that remains is also a fraction, say $v$, of that total kinetic energy. This, in turn, implies (using the relation to $K$ in (8.3) and (2.4)) that the maximum volumetric radius achieved after the rebound will be $v^{1/3}$ of that achieved before the collapse. If $v$ is some moderate fraction, this implies that only a very small number of collapse and rebound cycles will be observed. Experimental observations such as those of Ellis (1952), Lauterborn & Bolle (1975), Vogel, Lauterborn & Timm (1989) and Tomita & Shima (1990) clearly show that the number of rebounds usually lies between one and three. The plots of Shima & Tomita (1981), for example, suggest that $v^{1/3}$ lies between 0.5 and 0.3, which yields values of $v$ between 0.03 and 0.1. Clearly, to quantify this process more accurately requires considerably more information than can be developed here. However, it is encouraging to recognize that the analysis is qualitatively consistent with the experimental observations.

Before leaving the subject, the other drain for kinetic energy, namely the additional surface free energy, $E_S$, in the fission fragment cloud, should be briefly examined. Provided the number of fragments is much larger than unity:

$$E_S \approx 4\pi S R_F^2 n_m^3 = 4\pi S R_*^2 n_m \approx 4\pi S R_{min}^2 n_m, \tag{8.4}$$

where $n_j$ is an alternative to $n_m$. It follows from (8.4) and (7.3), using earlier expressions for $R_{min}$ and $K$, that

$$\mu_e = \tfrac{9}{16}(k+1)^{3/2}(\sigma + 2/R_o^*)^{1/2(k-1)} C_Q^{-3k/2(k-1)} \{2(p_\infty^i - p_\infty^m)/3\rho\}^{-1/2} S n_m. \tag{8.5}$$

Then taking, as an example, (3.5) for $n_m$, and omitting some constants of order unity, the resulting effective viscosity becomes

$$\mu_e = (\sigma + 2/R_o^*)^{1/6(k-1)} C_Q^{-1/2(k-1)} \{\rho R_o S\}^{1/2}. \tag{8.6}$$

Examine now the order of magnitude of the effective viscosity predicted by (8.6). Since the order of magnitude of the other terms is of order unity, the primary contribution is the value of $\{\rho R_o S\}^{1/2}$. For nuclei of size $R_o = 10\,\mu\text{m}$ and $100\,\mu\text{m}$, respectively, in water, this primary contribution takes values equal to $0.025\,\text{kg m}^{-1}\,\text{s}^{-1}$ and $0.08\,\text{kg m}^{-1}\,\text{s}^{-1}$, respectively. In comparison, the dynamic viscosity of water is about $0.001\,\text{kg m}^{-1}\,\text{s}^{-1}$. Thus, the fission surface free-energy contribution to the effective viscosity is close to two orders of magnitude larger than that of the liquid viscosity in the spherically symmetric model. A very similar result is obtained if one chooses to use $n_j$ rather than $n_m$ in (8.5). However, more importantly, this fission surface free-energy contribution still appears to be small compared with the mixing contribution discussed first.

In summary, I find that both the absorption of energy into surface free energy as a result of fission and the dissipation of energy owing to the mixing produced by the non-spherically symmetric motions are much larger than the traditional liquid viscosity contribution to the damping. However, for typical applications to cavitation resulting from micrometre-sized nuclei in water, the mixing contribution dominates the surface free-energy contribution. Only a qualitative examination of this dominant contribution has been attempted in this paper and it suggests a specific ratio of the maximum bubble size after collapse to that before. At present, it therefore seems practical to examine the experimental observations for an appropriate value of this ratio and to use this in the Rayleigh–Plesset module in larger codes.

## 9. Conclusions

Spurred by the need for multiphase flow models of cavitating flows which incorporate accurate Rayleigh–Plesset models for the bubble dynamics, this paper has examined one of the deficiencies in the Rayleigh–Plesset calculations which occur during cavitating bubble collapse. Numerous experimental observations have revealed that though a single coherent bubble may enter the very rapid collapse phase, almost invariably what emerges is either a highly distorted bubble or a cloud of smaller bubbles. This paper seeks to elucidate this fission process and begins by qualitatively evaluating the number of fission fragments that would result from (i) a fission process resulting from a Rayleigh–Taylor instability of the interface and (ii) a fission process resulting from a re-entrant jet collapse mechanism. Both mechanisms lead to qualitatively similar fission fragment numbers that depend on several global parameters which are identified.

In seeking some experimental verification of these fission fragment numbers I turn, not to pictures of cavitation bubbles (which do not, as yet, have the resolution that would allow the counting of bubbles), but to the photographs by Shepherd, Frost and Sturtevant of the fission of collapsing ether vapour bubbles in glycerol. The theory and observation of the number of fission fragments are qualitatively similar. However, the observed number of fragments is significantly smaller perhaps because viscous effects on the instability were not incorporated in the theory.

The paper ends by evaluating how the fission process will contribute to the damping of the global volumetric motions that the Rayleigh–Plesset equation is often used to simulate. It is shown that the kinetic energy that is dissipated by the mixing and turbulence associated with fission is much greater than the energy which is deflected into the additional free-surface energy. However, both are much greater than the energy dissipated by the classical viscous, thermal and acoustic mechanisms normally used to evaluate the bubble damping. Thus, the paper concludes that for a Rayleigh–Plesset method to model the global volumetric motions of the bubble or bubble cloud adequately, it is neccessary to introduce an energy dissipation mechanism associated with the fission process. The analysis shows that, at present, the best way to do this is to set the kinetic energy emerging from the collapse to some fraction of that entering collapse. However, comparisons with experimental observations are neccessary to establish the best value for that fraction.

This paper is dedicated to the memory of my colleague Brad Sturtevant whose enthusiasm and dedication inspired all who knew him. I would also like to thank Joe Shepherd, David Frost, Tim Colonius and Steve Hostler for their contributions to this paper.

## REFERENCES


BIRKHOFF, G. 1954 Note on Taylor instability. *Q. Appl. Maths* **12**, 306–309.

BLAKE, J. R. & GIBSON, D. C. 1987 Cavitation bubbles near boundaries. *Annu. Rev. Fluid Mech.* **19**, 99–124.

BRENNEN, C. E. 1995 *Cavitation and Bubble Dynamics.* Oxford University Press.

CHAPMAN, R. B. & PLESSET, M. S. 1971 Thermal effects in the free oscillation of gas bubbles. *Trans. ASME: J. Basic Engng* **93**, 373–376.

ELLIS, A. 1952 Observations on cavitation bubble collapse. Rep. no. 21-12, Hydrodynamics Laboratory, California Institute of Technology.

FROST, D. 1985 Effects of ambient pressure on the instability of a liquid boiling explosively at the superheat limit. PhD thesis, California Institute of Technology.

FROST, D. & STURTEVANT, B. 1986 Effects of ambient pressure on the instability of a liquid boiling explosively at the superheat limit. *Trans. ASME C: J. Heat Transfer* **108**, 418–424.

HILGENFELDT, S., BRENNER, M. P., GROSSMANN, S. & LOHSE, D. 1998 Analysis of Rayleigh–Plesset dynamics for sonoluminescing bubbles. *J. Fluid Mech.* **365**, 171–204.

KUHN DE CHIZELLE, Y., CECCIO, S. L. & BRENNEN, C. E. 1995 Observations and scaling of travelling bubble cavitation. *J. Fluid Mech.* **293**, 99–126.

LAUTERBORN, W. & BOLLE, H. 1975 Experimental investigations of cavitation bubble collapse in the neighbourhood of a solid boundary. *J. Fluid Mech.* **72**, 391–399.

MATSUMOTO, Y. & TAKEMURA, F. 1994 Influence of internal phenomena on gas bubble motion. *JSME Intl J.* **37**, 288–296.

NIGMATULIN, R. I., KHABEEV, N. S. & NAGIEV, F. B. 1981 Dynamics, heat and mass transfer of vapour–gas bubbles in a liquid. *Intl J. Heat Mass Transfer* **24**, 1033–1044.

PLESSET, M. S. & MITCHELL, T. P. 1956 On the stability of the spherical shape of a vapour cavity in a liquid. *Q. Appl. Maths* **13**, 419–430.

PROSPERETTI, A. 1991 The thermal behaviour of oscillating gas bubbles. *J. Fluid Mech.* **222**, 587–616.

SHEPHERD, J. E. 1980 Dynamics of vapour explosions: rapid evaporation and instability of butane droplets exploding at the superheat limit. PhD thesis, California Institute of Technology.

SHEPHERD, J. E. & STURTEVANT, B. 1982 Rapid evaporation at the superheat limit. *J. Fluid Mech.* **121**, 379–402.

SHIMA, A. & TOMITA, Y. 1981 The behaviour of a spherical bubble near a solid wall in a compressible liquid. *Ing. Arch.* **51**, 243–255.

TOMITA, Y. & SHIMA, A. 1990 High-speed photographic observations of laser-induced cavitation bubbles in water. *Acustica* **71**, 161–171.

VOGEL, A., LAUTERBORN, W. & TIMM, R. 1989 Optical and acoustic investigations of the dynamics of laser-produced cavitation bubbles near a solid boundary. *J. Fluid Mech.* **206**, 299–338.